This is the accepted manuscript made available via CHORUS. The article has been published as:

Droplet impact on vibrating superhydrophobic surfaces

Patricia B. Weisensee, Jingcheng Ma, Young Hwan Shin, Junjiao Tian, Yujin Chang, William P. King, and Nenad Miljkovic

Phys. Rev. Fluids **2**, 103601 — Published 9 October 2017

DOI: 10.1103/PhysRevFluids.2.103601

Droplet impact on vibrating superhydrophobic surfaces

Patricia B. Weisensee[1*], Jingcheng Ma[1*], Young Hwan Shin[1], Junjiao Tian[1], Yujin Chang[1], William P. King[1+], and Nenad Miljkovic[1,2+]

[1]*Department of Mechanical Science and Engineering, University of Illinois at Urbana-Champaign, USA*

[2]*International Institute for Carbon Neutral Energy Research (WPI-I2CNER), Kyushu University, 744 Motooka, Nishi-ku, Fukuoka 819-0395, Japan*

[*] *These authors contributed equally to the work*

[+] *Corresponding authors:*

nmiljkov@illinois.edu, (001)-617-981 9247, Mechanical Engineering Laboratory, 105 South Mathews Av., Urbana, IL 61801, USA

wpk@illinois.edu, (001)-217-244 3864, Mechanical Engineering Laboratory, 105 South Mathews Av., Urbana, IL 61801, USA

ABSTRACT

Many unanswered questions remain pertaining to the droplet dynamics during water droplet impact on vibrating surfaces. Using optical high speed imaging, we investigate the impact dynamics of macroscopic water droplets (~ 2.5 mm) on rigid and elastic superhydrophobic surfaces vibrating at 60 – 320 Hz and amplitudes of 0.2 – 2.7 mm. Specifically, we study the influence of the frequency, amplitude, rigidity, and substrate phase at the moment of impact on the contact time of impacting droplets. We show that a critical impact phase exists at which the contact time transitions from a minimum to a maximum greater than the theoretical contact time on a rigid, non-vibrating superhydrophobic surface. For impact at phases higher than the critical phase, contact times decrease until reaching a minimum of half the theoretical contact time just before the critical phase. The frequency of oscillation determines the phase-dependent variability of droplet contact times at different impact phases: higher frequencies (> 120 Hz) show less contact time variability and have overall shorter contact times compared to lower frequencies (60 – 120 Hz). The amplitude of vibration has little direct effect on the contact time. Through semi-empirical modeling and comparison to experiments, we show that phase-averaged contact times can increase or decrease relative to a non-vibrating substrate for low (< 80 Hz) or high (> 100 Hz) vibration frequencies, respectively. This study not only provides new insights into droplet impact physics on vibrating surfaces, but also develops guidelines for the rational design of surfaces to achieve controllable droplet wetting in applications utilizing vibration.

I. INTRODUCTION

The dynamics of droplets impacting rigid surfaces [1,2], soap films [3,4] and liquids [5–8] have been widely studied due to their high importance in both nature [9,10] and industry [11–13]. Despite the ubiquitous occurrence of droplet impact on vibrating surfaces in the mid-frequency range of $f = 50 – 500$ Hz, such as on turbine blades [14], pumps and compressors [15], insect wings [16], automotive systems [17], and fragmentation and dispersion systems [18], very few studies have characterized the droplet dynamics during such impact conditions. On vibrated liquid baths, droplet dynamics and droplet bouncing have been shown to strongly depend on the relationship between the vibration frequency and the droplet eigenfrequency [7], as well as the vertical acceleration of the bath [19]. During droplet impact on heated copper plates, low frequency, high amplitude vibrations at 100 – 250 Hz and accelerations of $a \sim 10^3$ m/s² = 100 g in the direction of the falling droplet can suppress the Leidenfrost effect [20]. At these high substrate accelerations, the collision force between droplet and substrate increases, allowing droplets to contact the hot plate, resulting in nucleate boiling rather than film boiling (Leidenfrost effect). For temperatures lower than the Leidenfrost temperature (≈ 170°C for water on static plates), spreading dynamics and the maximum spreading diameter are independent of substrate vibration [18]. However, vibrations at $f = 80 – 200$ Hz can enhance secondary fragmentation of fingers near the point of maximum droplet spreading. The resulting satellite droplets have diameters similar to the characteristic size of the fingers during natural impact without vibrations [18]. Non-vibrating, yet motion controlled targets influence droplet rebound [21]. Properly timed reversal of vertically moving substrates can suppress or promote droplet rebound on flat hydrophobic polymer surfaces, depending on the direction of substrate motion and speed. When the direction of an originally downward moving target reverses during droplet

impact, droplet rebound is enhanced. Similarly, when the substrate movement changes from up to down upon impact, droplet rebound is suppressed [21]. The initial qualitative explanation did not contribute the change in rebound behavior to an effective change in net impact speed. Rather, it suggested that a coupling of kinematic and dynamic effects, and consequently a comparison of time scales, influences droplet rebound. Droplet rebound enhancement (sinusoidal and triangular waveforms) and suppression (square waveform) have also been demonstrated for impact on horizontally oscillating surfaces [22]. Rebound suppression was caused by an interference of velocity fields within the droplet during the recoil phase. Due to the non-slip boundary condition at the droplet-substrate interface, the horizontal velocity field of the substrate oscillation superimposes the natural vertical velocity field within the droplet that is responsible for droplet lift-off. Droplets stretch and elongate in one preferential direction, losing their spreading symmetry and the ability to completely rebound [22]. To our knowledge, no study has been published that examines the influence of vertical solid substrate oscillations on droplet impact dynamics.

Here, we study the effect of vertical sinusoidal substrate vibrations at 60 – 320 Hz and amplitudes of 0.2 – 2.7 mm on the contact times and splashing behavior of droplets impacting superhydrophobic rigid and elastic surfaces. Through high-speed imaging and semi-empirical mathematical modeling, we describe the relationship between contact time and vibration frequency, phase, amplitude, and rigidity of the substrate. We provide new insights into droplet impact physics on vibrating surfaces and develop guidelines for the rational design of surfaces to achieve controllable droplet wetting in applications utilizing vibration.

II. EXPERIMENTAL SETUP

To represent a wide range of realistic impact scenarios in both industry and nature, we used two substrate configurations: (a) vibrating rigid substrate, and (b) vibrating elastic substrate in a cantilever mount. Figure 1 shows the experimental setup of the two configurations. In all cases, de-ionized (DI) water was supplied to a 25 gauge needle from a gravity bag (Enteral Feeding Gravity Bag, Dynarex) attached to the ceiling of the room (≈ 1.5 m above the sample). Droplets with diameters $D_0 \approx 2.5$ mm formed at the tip of the needle and impacted the substrate from a height h, resulting in speeds v = 1.20 – 1.35 m/s of the falling droplet upon impact (absolute velocity), corresponding to Weber, Reynolds, and Capillary numbers of $We = \rho v^2 D_0/\gamma$ = 50 – 65, $Re = \rho v D_0/\mu$ = 3000 – 3400, and $Ca = \mu v/\gamma \approx 0.02$, respectively, where ρ, γ, and μ are the density, surface tension, and dynamic viscosity of water, respectively. A high speed camera (Phantom v711, Vision Research), coupled to a 1-5x macro lens (Canon), recorded the impacting droplets at frame rates of 9,500 and 13,000 frames per second (fps) and resolutions of 1024x768 and 800x600 pixels, respectively. A fiber-optic cable connected to a light source (EKE 150W, Kramer Scientific) provided sufficient back-lighting to achieve an exposure time of 10 – 30 μs. The images were calibrated with respect to the outer diameter of the dispensing needle, obtaining a resolution of 17 – 19 μm/pixel, resulting in a droplet size uncertainty of ± 0.2 mm and an impact speed uncertainty of ± 0.05 m/s. The images were analyzed with a custom written Matlab code to determine the initial diameter, impact speed, substrate frequency, amplitude, and phase of impact, while manual analysis was used to obtain contact times (measurement uncertainty: ± 0.2 ms). The uncertainty in impact phase is ±2°. Additional uncertainties due to surface inhomogeneity, deviations from a spherical shape upon droplet impact, as well as air flow irregularities are expected to occur [23–25]. To render the samples superhydrophobic, the

commercially available superhydrophobic coating NeverWet was sprayed onto a microscope slide (rigid substrate) and 100 μm thin polyhydroxybutyrate (PHB) polymer sheets (Goodfellow) (elastic substrate). The length and width of the elastic substrate were 15 mm and 8 mm, respectively, leading to a bending stiffness of 6 N/m. The inset in Fig. 1(a) shows a scanning electron microscopy (SEM) image of the nanoparticle coating. The apparent advancing and receding contact angles in the non-wetting Cassie-Baxter state were measured to be $\theta_A^{app}/\theta_R^{app}$ = 164 ± 4°/159 ± 3°. A detailed characterization of the coating can be found elsewhere [26].

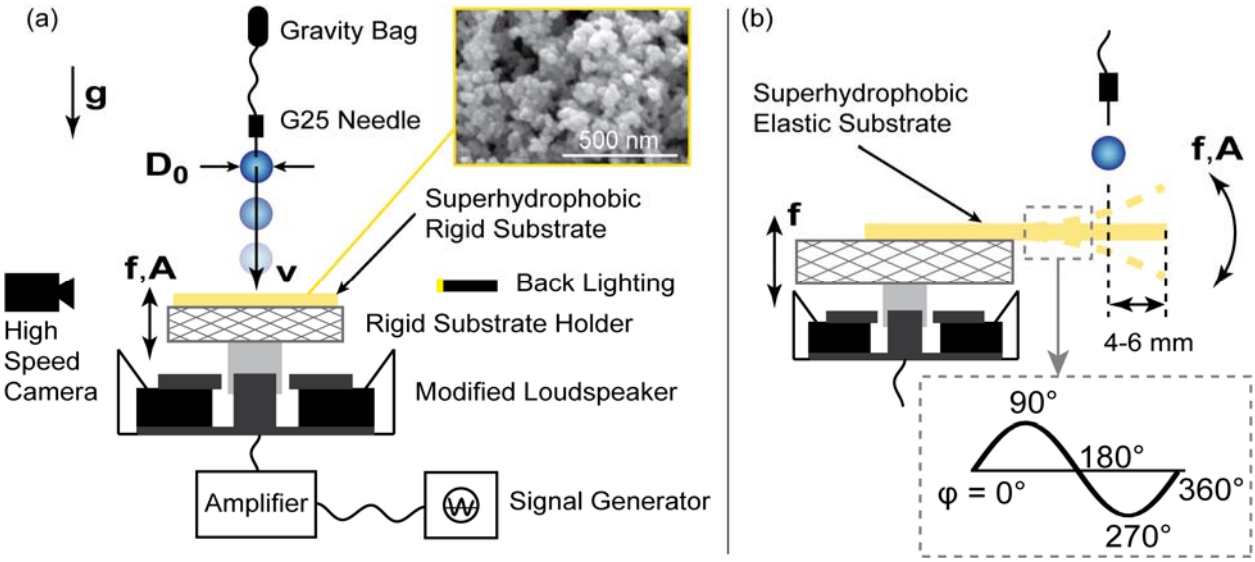

FIG. 1. Experimental setup and substrate configurations. (a) Droplets formed at the tip of a single needle and fell onto the substrate with a droplet diameter D_0 (2.5 mm) and an impact speed v (1.20 – 1.35 m/s). A high speed camera recorded the impact and the substrate motion (frequency f, amplitude A). The rigid superhydrophobic nano-textured substrate was mounted on a modified loudspeaker, which was connected to a sinusoidal wave form generator and signal amplifier. (b) An elastic superhydrophobic substrate was attached to the same loudspeaker configuration with a cantilever-mount.

Samples were mounted on a modified loudspeaker system. A laptop generated sinusoidal acoustic waves with frequencies f = 60 – 320 Hz that were transferred to a micro stereo amplifier (TDA7297, DROK) using a standard audio cable. The amplified signal was the input to a multimedia speaker (2□, 4Ω 12W Stereo Audi Speaker, DROK), modified by removing the

cover and cone to place a rigid substrate holder directly onto the vibrating voice coil. All reported frequencies were experimentally measured using high speed imaging. The measured amplitudes, defined as the half distance between the two vibration extrema, varied between A = 0.2 – 2.7 mm. Figure 1(a) shows the setup for the rigid vibrating sample, where a superhydrophobic coated glass slide was placed directly on the rigid substrate holder. Figure 1(b) depicts the setup for the elastic vibrating sample, where a thin superhydrophobic polymer sheet was mounted on the substrate holder with adhesive electrical tape, protruding on one side, resulting in a cantilever mount. Individual droplets impacted within 4-6 mm from the free end of the cantilever substrate, such that during initial spreading, the droplets would not spread over the edge of the substrate. We did not observe twisting of the substrate during impact. Vibration amplitudes were characterized at the location of impact. We define the polar angle $\varphi = 0$ at the point of maximum upward substrate speed (see Fig. 1(b)).

The two different configurations allowed us to differentiate between strong and weak amplitudes and accelerations, as well as substrate response to droplet impact. To mimic impact on plant leaves we also studied the successive impact of water droplets on stationary elastic substrates. Experimental setup and results on these passively vibrating surfaces can be found in sections S2 and S3 of the supplementary information [27].

III. RESULTS AND DISCUSSION

A. Observations of droplet dynamics

We first considered droplet impact on rigid superhydrophobic surfaces. We found that droplet dynamics and contact times can vary significantly, depending on the phase of the substrate vibration at the moment of impact, defined herein as the impact phase. Substrate

frequency and amplitude played only a minor role in altering droplet dynamics. Figure 2 shows optical images of rebounding droplets under various impact conditions.

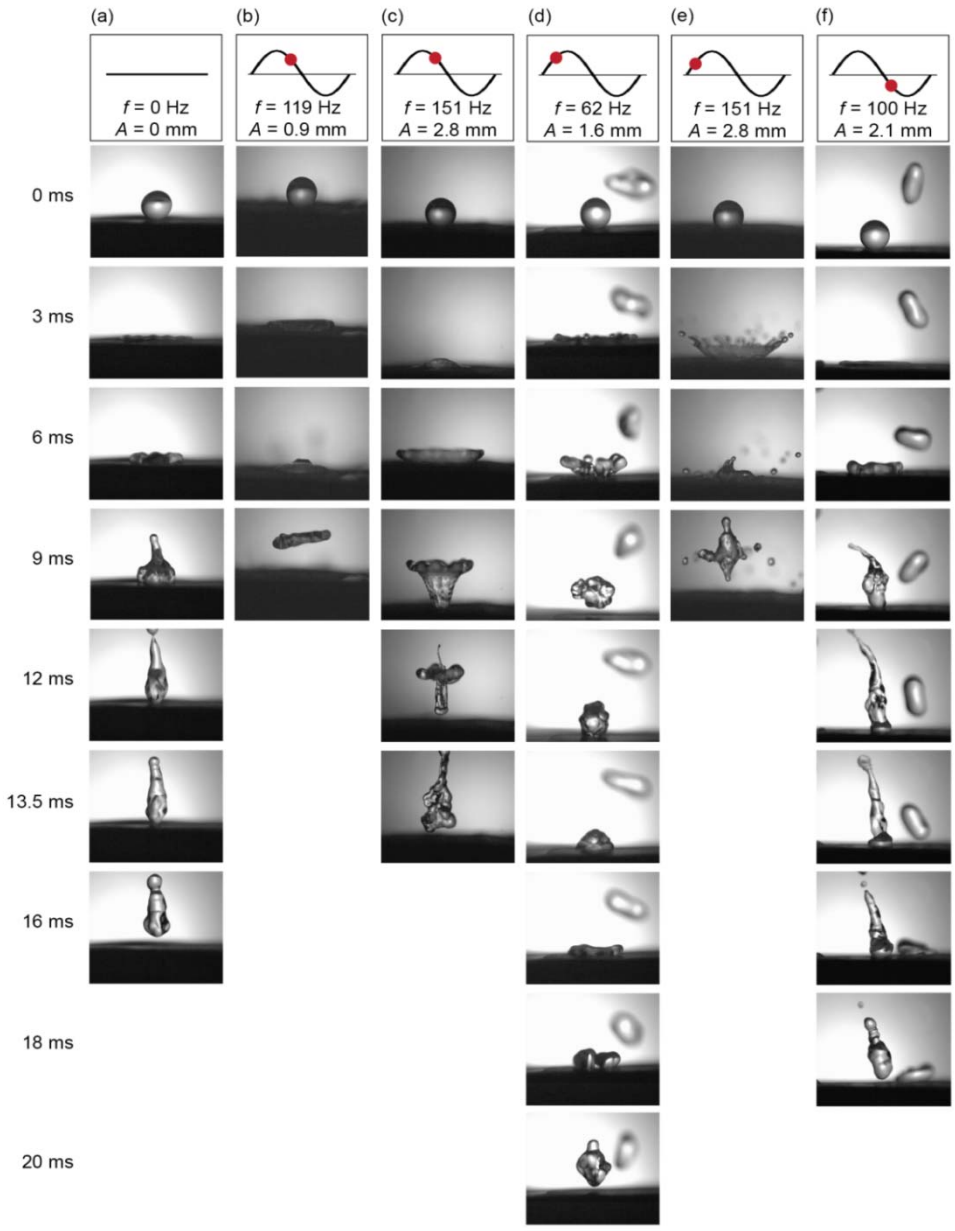

FIG. 2. Droplet shapes for various impact conditions ($D_0 \approx 2.5$ mm, $v = 1.35$ m/s) during impact on rigid superhydrophobic surfaces**.** (a) Impact on a stationary substrate with traditional spreading, recoil and lift-off at the theoretical contact time $t_{c,th}$. (b)-(f) Impact on vibrating substrates. A red dot marks the impact phase. (b) Impact just below the critical impact phase led to pancake bouncing and the shortest contact times $t_c \approx t_{c,th}/2$. (c) At higher amplitudes, a superposition of pancake bouncing and crown splashing, called tulip splashing, occurred during the substrate upward movement. (d) At phases smaller than the critical phase, the substrate caught up with the departing droplet after initial pancake bouncing and caused droplet re-attachment. (e) Crown splashing occurred when the

droplet deceleration was greater than a critical value upon impact. (f) Impact just above the critical phase led to long jets and the longest contact times $t_c > t_{c,th}$.

Droplets impacting a stationary reference sample (Fig. 2(a)) displayed the traditional spreading, recoil and lift-off mechanism governed by the inertial-capillary scaled contact time (herein called the theoretical contact time) [28]:

$$t_{c,th} = 2.6\sqrt{\frac{\rho D_0^3}{8\gamma}}. \quad (1)$$

For droplets with an initial diameter D_0 = 2.5 mm, the theoretical contact time is $t_{c,th}$ = 13.5 ms. It should be noted that the contact time on stationary rigid hydrophobic surfaces is independent of impact speed [2,28]. As opposed to previous experiments on droplet impact on vibrating baths, where droplet sizes and impact speeds were small (We < O(1)) and thus droplet deformations during impact were minimal, in the present experiments we observed significant droplet spreading and capillary waves at the droplet liquid-vapor interface [7,19]. Figure 2(b) shows a droplet with the shortest possible contact time with $t_c \approx t_{c,th}/2$. In the example shown, the droplet underwent pancake bouncing, where the droplet lifted off the surface near maximum spreading without recoil, similar to the recently discovered springboard effect on elastic substrates [26]. As we will show later, contact time minimization is associated with impact at a critical phase. Impact at the same phase, but with higher vibration amplitudes, resulted in a superposition of pancake bouncing and crown splashing (Fig. 2(c)). The droplet rim detached while the momentum of the center of the droplet was still downward and the droplet thus remained in contact with the substrate. Due to the resemblance of the droplet shape to a calyx, we call this droplet bouncing mechanism *tulip-splashing*. In some cases, when droplets impacted at a phase smaller than the critical phase, we first observed pancake bouncing, with the vibrating substrate catching up with the departing droplet, resulting in droplet re-attachment and another, more

chaotic, impact cycle (Fig. 2(d)). The combined contact time of first and second impact cycle was longer than the theoretical contact time. Impact at a similar phase, but higher vibration frequency and amplitude led to crown splashing with greatly reduced contact times (Fig. 2(e)). Impact slightly after the critical phase also increased contact times. Initial droplet spreading and recoil were similar to those on a stationary substrate; however, the liquid jet remained in contact with the substrate and droplet lift-off was delayed, as shown in Fig. 2(f). Video S1 of the supplementary information shows the six droplet impact cases [27]. In addition to these six droplet behaviors, we observed many hybrid shapes for slightly varying impact conditions, which are not discussed here in detail.

After characterizing the different modes of droplet dynamics for impact on vibrating rigid surfaces, we next turn to vibrating elastic surfaces. Droplet dynamics and contact times are similar to those on vibrating rigid surfaces. Figure 3 shows the experimentally measured substrate deflection δ along with optical images to illustrate droplet and substrate dynamics for three different impact conditions. Figure 3(a) shows a droplet impacting the vibrating substrate at φ = 295°, near the bottom dead center of substrate vibration, such that the impact has little influence on the vibration of the substrate. With substrate vibration at f = 60 Hz and A = 2.7 mm, the droplet impacted the substrate just prior to the critical phase $\varphi \lesssim \varphi_c$ = 316°. The droplet spread and lifted off in a pancake shape, with a contact time shorter than the theoretical contact time ($t_c < t_{c,th}$). When the droplet impacted the substrate at $\varphi > \varphi_c$, as shown in Fig. 3(b) for f = 60 Hz and A = 1.4 mm, it first spread and then elongated vertically, forming a jet-like shape. When the substrate moved upwards, the droplet compressed. Finally, near the substrate top dead center, the droplet lifted off at $t_c > t_{c,th}$. Figure 3(c) shows the dynamics of a splashing droplet impacting at φ = 326° on a substrate with f = 120 Hz and A = 2.0 mm. The substrate vibrated as a

cantilever, i.e. the droplet impacted an inclined surface for $\varphi \neq 0, 180°$. Due to a faster vertical acceleration away from the substrate mount, the droplet splashing symmetry was broken and satellite droplets ejected preferentially at the side facing the substrate free end where acceleration was maximum and the slope of inclination highest. The remaining droplet core lifted off in a pancake-like shape. A similar non-symmetric splashing has been observed for impact on plant leaves [9], and for oblique droplet impact [29–31]. Video S2 of the supplementary information shows the three droplet impact cases [27].

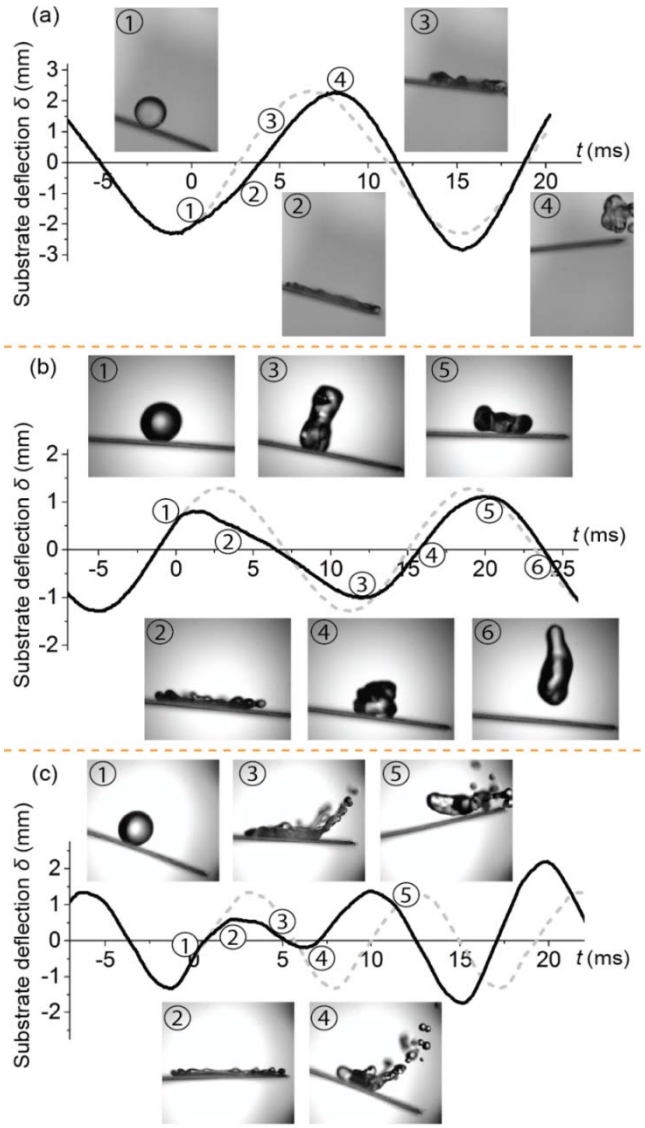

FIG. 3. Substrate deflection and droplet shapes for various impact conditions ($D_0 \approx 2.5$ mm, $v = 1.20$ m/s) on elastic superhydrophobic surfaces under forced vibration. The droplet impact influences the substrate movement on the elastic vibrating substrates. Solid black curves represent the actual substrate deflection, while the gray dotted lines represent the natural substrate vibration without impact. (a) Impact at $\varphi = 295°$ ($\varphi_c = 316°$) resulted in a reduced contact time ($t_c < t_{c,th}$) ($f = 60$ Hz, $A = 2.7$ mm). (b) Impact at $\varphi = 26°$ ($\varphi_c = 322°$) resulted in an elongated contact time ($t_c > t_{c,th}$) ($f = 60$ Hz, $A = 1.4$ mm). (c) The droplet splashed at $\varphi = 326°$ ($f = 120$ Hz, $A = 2.0$ mm).

When droplets impacted the substrate away from the top and bottom dead ends of vibration, as seen in Figs. 3 (b) and (c), they manipulated the substrate vibration. This secondary vibration, caused by the droplet impact, is similar to a bending wave that has been observed previously for droplet impact on flexible fibers [32]. Due to the strong external driving force in the present experiments, the original vibration is recovered within a few oscillation periods. The detailed substrate response was extremely complex, and dependent on the axial impact location, phase, frequency, amplitude. Droplet dynamics for other impact conditions were similar to those presented above and mainly depended on the impact phase and its relation to the critical impact phase. Vibration frequency and amplitude affected the likelihood of splashing, but had little influence on the dynamics of non-splashing droplets [33,34] (see section S4 of the supplementary information [27]). We did not observe periodic droplet bouncing or resonance for impact on rigid or elastic substrates [35,36]. After lift-off, droplets were highly distorted and underwent chaotic dynamics. When droplets impacted the substrate for a second time, droplet dynamics varied strongly from those at first impact (quasi-spherical droplet) due to an overlaying contribution of internal and external velocity fields. The droplet resonance frequency in its first resonant mode (Y_2^0) for $D_0 = 2.5$ mm is $f_R = 86$ Hz [36,37]. Impact experiments at 80 and 100 Hz revealed that droplet dynamics and contact times did not differ from those at other vibration frequencies.

As seen from the images in Figs. 2 and 3, contact times and droplet dynamics are very sensitive to impact conditions. Figure 4(a) shows the normalized contact times, defined as the actual contact time divided by the theoretical contact time $t_c/t_{c,th}$, for all vibration frequencies and

amplitudes as a function of impact phase for rigid and elastic vibrating surfaces. At first glance, no clear correlation between contact time and frequency, amplitude, and phase exists. However, even from this rather chaotic plot we can identify two important findings: (1) all contact times are well bounded by $0.5t_{c,th} \leq t_c \leq 1.6t_{c,th}$, i.e. contact times can increase or decrease relative to the theoretical contact time on a stationary substrate, and (2) within small frequency ranges, contact times are mostly independent of vibration amplitude (± 7% variation). In light of the amplitude independence, we can combine data of similar vibration frequencies to obtain a clearer depiction of the trends, as shown in Fig. 4(b), for a subset of frequencies including all respective vibration amplitudes. For each frequency, contact times suddenly increase at certain impact phases and decrease monotonically thereafter (recall that 360° = 0° of the next vibration period). For frequencies of 60, 100, 120, and > 200 Hz, the discontinuity occurs at $\varphi \approx 20°$, 175°, 160°, and 100°, respectively. From Fig. 4(b), we also observe that average contact times decrease for an increase in vibration frequency, and that the jump at the discontinuity becomes smaller for higher frequencies, i.e. contact times become less dependent on the impact phase for increasing vibration frequencies. We attribute the scatter in data in Fig. 4(b) to the lumping of vibration amplitudes, minor differences in droplet size, and slight oscillations during free fall caused by the dispensing mechanism.

As observed in Fig. 4(a), vibration amplitudes in the range $A = 0.3 – 2.7$ mm have little effect on contact times. However, as the amplitude approaches zero, i.e. no vibration, contact times should approach $t_c = t_{c,th}$. In fact, experiments at $f = 151$ Hz and $A = 0.2$ mm reveal a physical limit to the variation of contact times *via* substrate vibrations, where contact times are at $t_c = 0.8 – 1.0\ t_{c,th}$ for all impact phases and do not show a discontinuity of contact times at a critical

impact phase (see gray triangles in Fig. 4(a)). Details on these limits will be discussed below in section B.

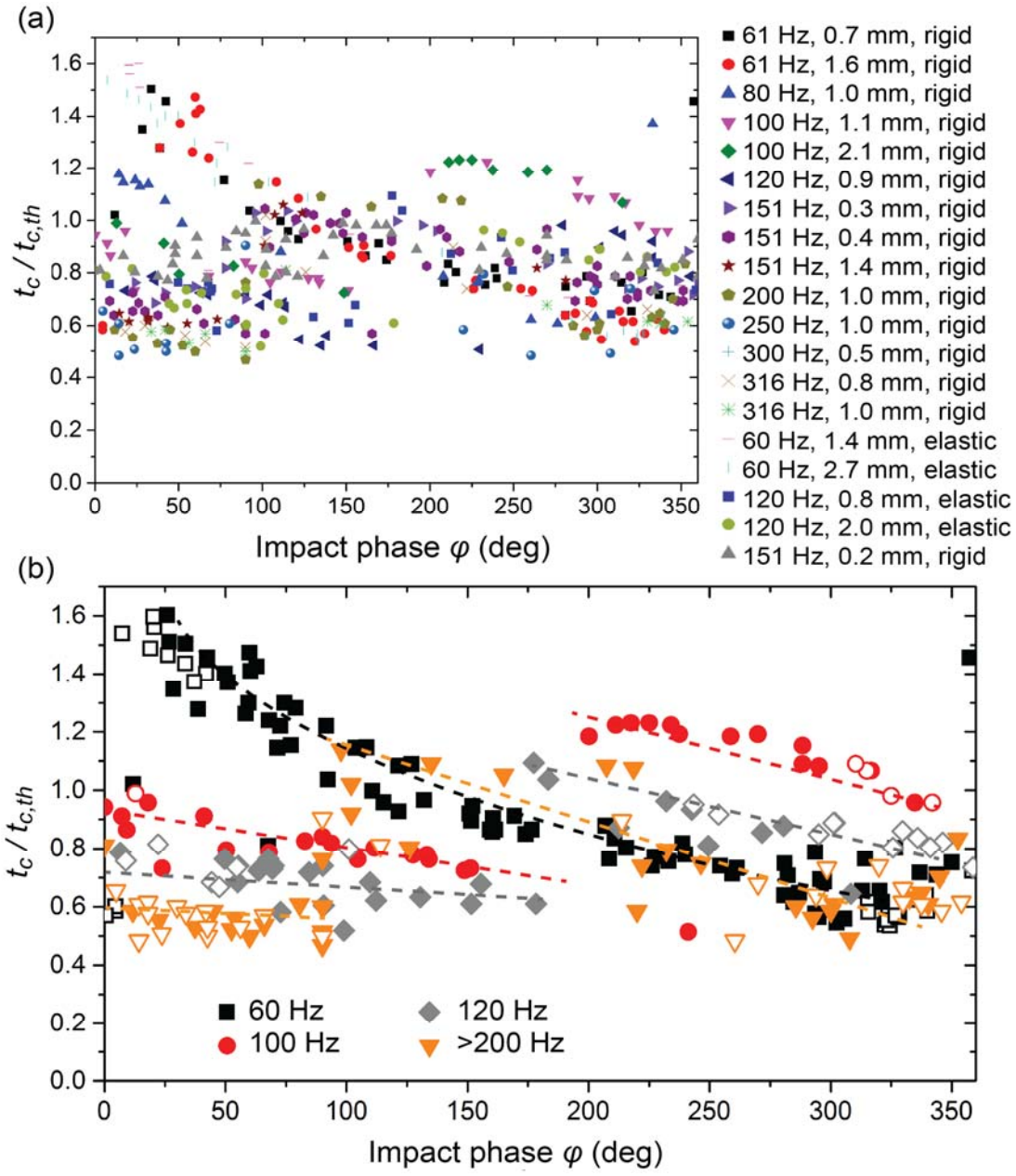

FIG. 4. Contact time analysis. (a) Normalized contact times as a function of impact phase on vibrating rigid and elastic superhydrophobic surfaces for all substrate vibration frequencies and amplitudes. Contact times show a small dependence on vibration amplitude (± 7%). (b) Sub-set of data from (a), where amplitudes for each frequency are combined for clarity. Dotted lines represent trend lines. For each frequency, contact times suddenly increase at a certain impact phase and decrease thereafter. Open symbols represent droplets that splashed during impact.

B. Mathematical modeling of contact times

To understand the origin of the discontinuity in contact times, we analyzed the interplay between substrate position and droplet dynamics in more detail. Figure 5(a) shows the distribution of departure phases for impacting droplets. Intuitively, one would expect droplets to lift off when the substrate is at its top dead center (90°), at the point when the substrate starts moving downward. Indeed, most droplets lifted off at phases between 80 and 180°, showing an average departure phase of $\varphi_d \approx 135°$ with a variation of approximately ± 90°. Physically, when the substrate moves upwards, it imparts vertical momentum to the spread droplet, initiating droplet lift-off. Due to droplet inertia, final droplet departure is delayed beyond $\varphi_d \approx 90°$, until the substrate moves downward, away from the droplet. In fact, when considering only those droplets that departed in a pancake shape with $t_c \approx t_{c,min}$, the average departure phase was 156°, indicating that the lift-off process is dominated by the downward motion of the substrate away from the droplet rather than an active *pushing* of the droplet upwards. With the quantification of a mean departure phase, we can now estimate the impact phase that would minimize contact times. Figure 4 revealed that the minimum contact time was $t_{min} \approx t_{c,th}/2$ [38–41] (see section S5 of the supplementary information for a detailed discussion on the nature of the minimum contact time [27]). The critical impact phase φ_c,when the discontinuity in contact time (Fig. 5(b)) occurs, can be defined as:

$$\varphi_c = \varphi_d - 2\pi f t_{\min}. \quad (2)$$

Comparison to experimental data confirms the linear dependence of φ_c with the vibration frequency, as shown in Fig. 5(b). Despite the larger variation in departure phase, Eq. (2) and experimental data show good agreement.

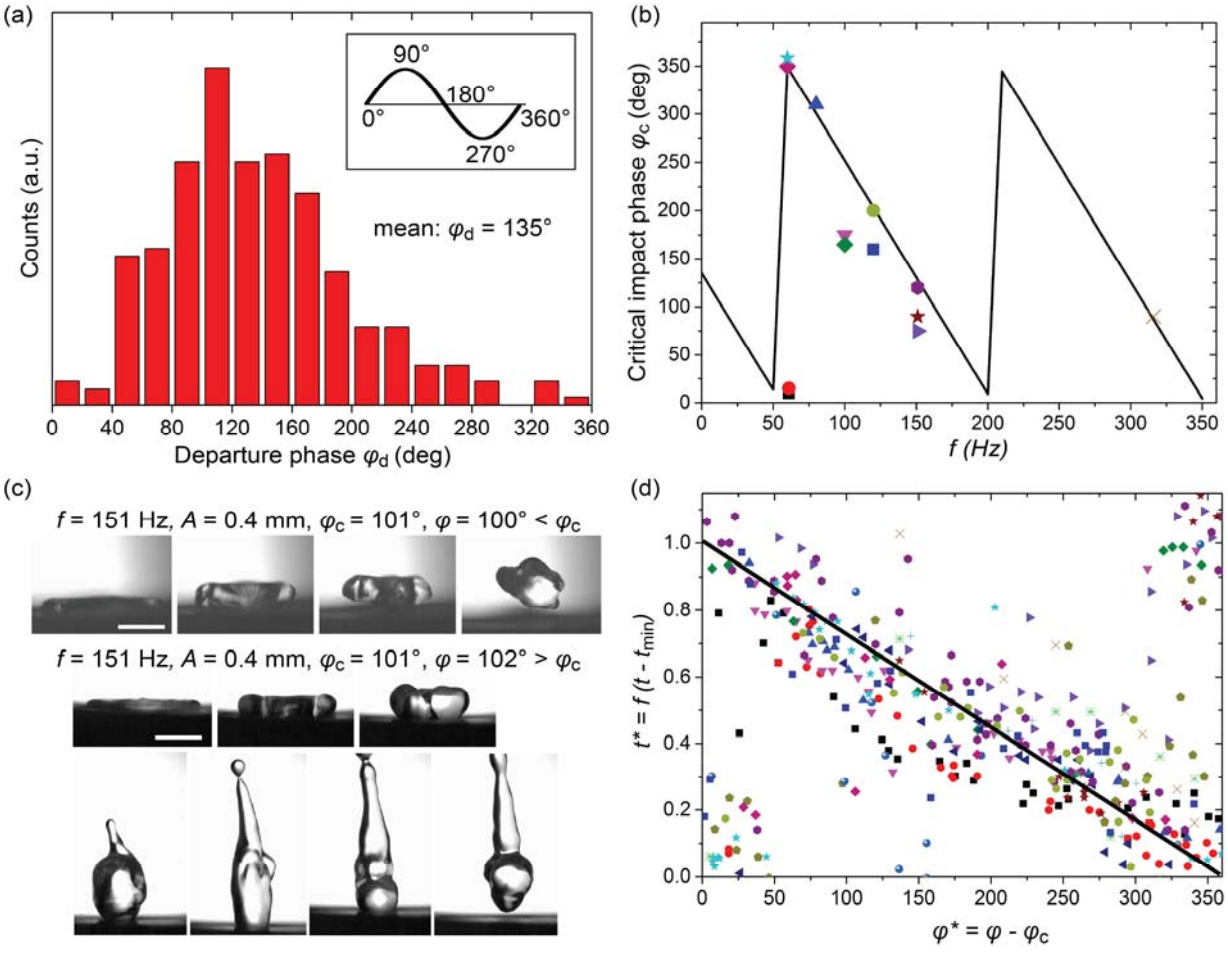

FIG. 5. Departure phase, critical impact phase and non-dimensional contact times for droplet impact on vibrating superhydrophobic surfaces. (a) Distribution of droplet departure phases. (b) Comparison of Eq. (2) to experimental data for the critical impact phase. (c) Droplet dynamics ($D_0 \approx 2.5$ mm, $v = 1.35$ m/s, $f = 151$ Hz, $A = 0.4$ mm, $\varphi_c = 101°$) for impact with $\varphi = 100° < \varphi_c$ (top) and $\varphi = 102° > \varphi_c$ (bottom) (scale bar 2 mm). The time step between each snapshot is 2 ms, respectively. (d) Non-dimensional contact times as a function of normalized impact phase with $\varphi_d = 135°$. The solid line represents Eq. (5). The legend for data points in (b) and (d) can be found in Fig. 4(a). Missing impact conditions in (b) did not have sufficient data points to determine φ_c.

Figure 5(c) compares droplet dynamics for impact phases approaching the critical impact phase from both sides. For impact just prior to the critical phase, contact times are minimized,

while droplets impacting at a later point cannot detach prior to the next full vibration period. Therefore, for the vibration frequencies (60 – 320 Hz) and amplitudes (0.3 – 2.5 mm) examined in this study, the maximum contact time can be approximated by

$$t_{max} = t_{min} + \frac{n}{f}, \tag{3}$$

where n is the number of periods that the substrate undergoes before droplet lift-off. For most cases studied here, n = 1. However, for higher frequencies (f > 250-300 Hz), n > 1. The vibration can cause the droplet to re-attach during recoil. However, during the next vibration cycle, the droplet would finally detach. Thus, the maximum possible contact time should be bound by $t_{max} \leq 2t_{c,th}$. This maximum contact time poses a constraint at the minimum vibration frequency f_{min} of the substrate, i.e. $f_{min} = 2/(3t_{c,th})$. For $f < f_{min}$, the droplet time scale for natural recoil is smaller than the vibration period, and the droplet lifts off at its theoretical contact time. For D_0 = 2.5 mm, we find that f_{min} = 50 Hz, which is just below the vibration frequencies tested in this work. From observations (Fig. (4(a)) $t_{max} \approx 1.75t_{c,th}$, which would correspond to f_{min} = 59 Hz.

Assuming that contact times vary linearly with impact phase we can write for $f > f_{min}$ and $A > A_{min}$, where A_{min} is the smallest vibration amplitude necessary to provide sufficient momentum for early droplet liftoff:

$$t = t_{max} - \frac{\varphi - \varphi_c}{2\pi f}. \tag{4}$$

For $f < f_{min}$ and $A < A_{min}$, the contact time is independent of vibration frequency and amplitude and approximately equal to the theoretical contact time, i.e. $t \approx t_{c,th}$.

Due to the periodicity of the vibration we introduce a normalized impact phase which includes the modulus of one vibration period, $\varphi^* = [(\varphi - \varphi_c), (mod\ 2\pi)]$, and a non-dimensional contact time $t^* = f\ (t - t_{min})$. Equation (4) then becomes:

$$t^* = 1 - \frac{\varphi^*}{2\pi}. \quad (5)$$

Figure 5(d) compares the experimental data with Eq. (5). The good agreement between model and data (standard deviation for all data: 30%) supports our hypothesis of a critical impact phase at which contact times transition from a minimum to a maximum. The scatter in data in the upper right and lower left corners arises from deviations of the actual departure phase from φ_d = 135°.

Previous studies of droplet impact on vibrating baths indicated the importance of the dimensionless peak acceleration $\Gamma = 4\pi^2 A f^2/g$, where g is the acceleration due to gravity, on droplet dynamics and rebound [7,19,36,42,43]. However, we did not observe a direct coupling between contact times and substrate acceleration. Even for the limiting case of f = 151 Hz and A = 0.2 mm, Γ = 18 >> 1. However, as we have shown previously, contact time reduction during impact on elastic substrates depends on the momentum transfer between the substrate and the spread droplet [26]. In the present work, we can adapt the Froude number criterion $Fr = u_s / (g D_{max})^{1/2} \geq 1$, where $u_s = 2\pi A f$ is the maximum substrate velocity, and D_{max} is the maximum droplet spreading diameter. For D_0 and v = 1.35 m/s, we find that $D_{max} \approx 6.1$ mm [26]. From the Froude number criterion, the frequency-dependent minimum vibration amplitude A_{min} can be determined. For f = 151 Hz, we find A_{min} = 0.26 mm, which is in excellent agreement with the observed transition between 0.2 and 0.3 mm.

To better understand the interplay between vibration frequency, amplitude, impact phase, and contact time, we numerically modeled the average contact times, taking into account the probability for droplet impact at a certain phase, given vibration amplitude and frequency. For high vibration frequencies and amplitudes, the probability of the droplet hitting the substrate at a certain phase is not equally distributed. Approximating the droplet as a small solid sphere, and

assuming that the droplet makes contact with the substrate at phase φ, then the vertical distance between droplet and substrate prior to impact is $s = A - vt - Asin(2\pi ft + \varphi_0)$. At impact ($s$ = 0), and for $\varphi = \omega t + \varphi_0$, the position of φ_0 can then be determined to $\varphi_0 = v^*(\sin\varphi - 1) + \varphi$, where $v^* = A\omega/v$ is the normalized substrate velocity, which represents the impact probability as a function of substrate phase. The probability of droplet impact at phase φ can be defined as $p(\varphi) = 0$ for $\varphi_1 \leq \varphi \leq \varphi_2$, or $p(\varphi) = \frac{1}{2\pi}(v^* \cos\varphi + 1)$ for all other phases. The phase angles φ_1 and φ_2 are defined as $\varphi_1 = \cos^{-1}(-1/v^*)$ and $\varphi_2 + v^* \sin\varphi_2 = \sqrt{v^{*2} - 1} + \cos^{-1}(-1/v^*)$, respectively. The latter equation does not have an analytical solution, but can be solved numerically. Section S6 of the supplemental information discusses the probability distribution in more detail [27]. The phase-averaged contact time of an impacting droplet can then be calculated using:

$$\bar{t}(f, A) = \int_{\varphi_2}^{\varphi_1} t(\varphi) p(\varphi) d\varphi \,, \tag{6}$$

where the contact time $t(\varphi)$ is described by Eq. (4), using the modulus of $(\varphi - \varphi_c)$. Note that Eq. (6) is only valid in the limits of $f > f_{min}$ and $A > A_{min}$, as outlined above. For $f < f_{min}$ and $A < A_{min}$, the contact time equals the theoretical contact time, independent of impact phase.

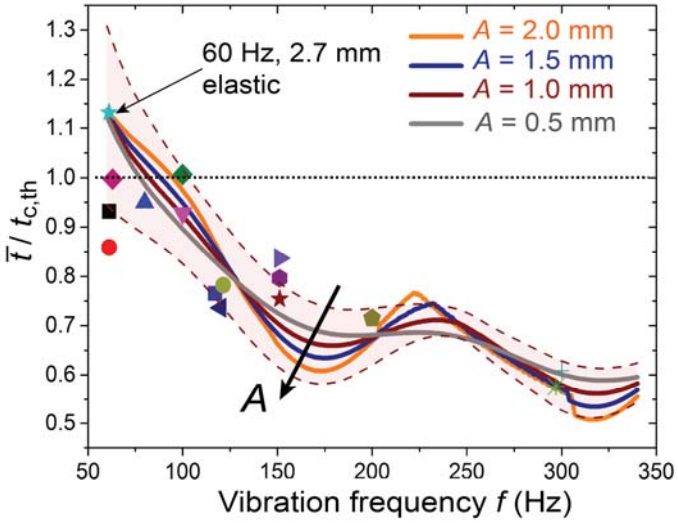

FIG. 6. Effect of vibration frequency, amplitude, and phase on contact times for droplet impact on vibrating superhydrophobic surfaces. Measured (points) and predicted (lines) average normalized contact times for droplet impact on rigid and elastic vibrating surfaces as a function of frequency and amplitude following Eq. (6). Shaded areas represent the uncertainty, as determined from the observed standard deviation between experimental data and Eq. (5) for A = 1 mm (SD = ± 30%). The legend for the data points can be found in Fig. 4(a). Note that the data point for 60 Hz, 2.7 mm, elastic, for which the experimental set is most complete across all impact phases, is directly at the intersection of the predicted model lines.

Equation (6) was solved numerically and is plotted in Fig. 6. The discontinuity in the average contact time for higher amplitudes arises from the impossibility of droplets to impact the substrate at certain vibrational phases. Overall, contact times decrease with increasing vibration frequency, and show local minima at $f \approx 170$ Hz and 320 Hz. Average contact times for vibration frequencies $f < 80$ Hz are higher than the theoretical contact time on a stationary rigid superhydrophobic substrate. For $f > 100$ Hz, contact times are reduced. The maximum possible average contact time enhancement is found to be $\overline{t_{max}}/t_{c,th} \approx 1.2$, independent of droplet size. From Fig. 6 we see that the transition frequency f_{trans} where $\bar{t}/t_{c,th} = 1$ (i.e. for $f < f_{\text{trans}}$, $\bar{t}/t_{c,th} > 1$ and for $f > f_{\text{trans}}$, $\bar{t}/t_{c,th} < 1$) depends slightly on the amplitude of the vibration. Section S7 of the supplementary information discusses the role of droplet size and fluid parameters on the average contact times and shows that f_{trans} is a function of droplet size, i.e. of the natural droplet oscillation frequency, and scales as $f_{\text{trans}} \sim a/t_{\text{c,th}}$, where $a = 1 - 1.3$ [27].

Figure 6 also includes the uncertainty in average contact times, as determined from the standard deviation between experimental data and Eq. (5). The uncertainty is more important for smaller vibration frequencies and decreases for increasing frequencies. Additionally, Fig. 6 also includes phase-averaged contact time data from Fig. 4(a). Qualitatively, data and model match well. Average contact times decrease with increasing vibration frequency, while the vibration amplitude has little effect on the average contact time. The discrepancy between data and model for the low vibration frequency of 60 Hz on the rigid substrates arises from the lack of data at

small impact phases, where local contact times would be highest. When averaging over a data set with contact time data for low and high impact phases, as is the case for the elastic substrates at f = 60 Hz and A = 2.7 mm, the model matches the data extremely well.

IV. CONCLUSIONS AND OUTLOOK

Using high speed imaging, we studied droplet dynamics and contact times during droplet impact on rigid and elastic vibrating superhydrophobic surfaces. We demonstrated that contact times can increase by 160% and decrease by 50% when compared to impact on stationary rigid superhydrophobic surfaces. Detailed analysis revealed that during forced vibration, the contact time is most sensitive to changes in the impact phase, whereas the amplitude of vibration had little direct effect on the contact time. We introduced the concept of a frequency-dependent critical impact phase at which contact times transitioned rapidly from a minimum ($t_c \approx 0.5t_{c,th}$) to a maximum ($t_c \approx 1.6t_{c,th}$). We show that the average contact time is frequency dependent, and can be greater (smaller) than the theoretical contact time for smaller (higher) frequencies. For a droplet diameter of 2.5 mm, the maximum average contact time occurs for vibrations of 50-60 Hz, and becomes smaller than the theoretical contact time for f > 80-100 Hz, depending on the amplitude of the substrate vibration. This study not only provides new insights into droplet impact physics on vibrating surfaces, but develops guidelines for the rational design of surfaces to achieve controllable droplet wetting in applications utilizing vibration.

In addition to providing rationale for the design of superhydrophobic surfaces for industrial applications, such as spray cooling, where the per droplet heat transfer rates increase (decrease) for longer (shorter) contact times, the aforementioned droplet impact dynamics on vibrating elastic surfaces have much potential to explain the evolved flexibility of natural

superhydrophobic surfaces, i.e. the wings of a butterfly or cicada, or the leaf of a plant. Although our work has focused on contact time and droplet dynamics, future studies should pay closer attention to Cassie-to-Wenzel or impalement transition during impact, and how surface flexibility and vibration affect these processes. Although recently studied on stationary flexible substrates [44], many natural superhydrophobic surfaces are not stationary and oscillate at frequencies ranging from few Hz (larger insects, plant leaves) [45] to hundreds of Hz (smaller insects) [46], giving rise to alternate dynamics during impact.

ACKNOWLEDGEMENTS

This work was supported by the National Science Foundation Engineering Research Center for Power Optimization of Electro Thermal Systems (POETS) with cooperative agreement EEC-1449548. N.M. gratefully acknowledges funding support from the Office of Naval Research (Grant No. N00014-16-1-2625). N.M. gratefully acknowledges the funding support of the International Institute for Carbon Neutral Energy Research (WPI-I2CNER), sponsored by the Japanese Ministry of Education, Culture, Sports, Science and Technology.

REFERENCES

[1] C. Josserand, S.T. Thoroddsen, Drop Impact on a Solid Surface, Annu. Rev. Fluid Mech. 48 (2016) 365–391. doi:10.1146/annurev-fluid-122414-034401.

[2] C. Antonini, A. Amirfazli, M. Marengo, Drop impact and wettability: From hydrophilic to superhydrophobic surfaces, Phys. Fluids 1994-Present. 24 (2012) 102104. doi:10.1063/1.4757122.

[3] T. Gilet, J.W.M. Bush, The fluid trampoline: droplets bouncing on a soap film, J. Fluid Mech. 625 (2009) 167. doi:10.1017/S0022112008005442.

[4] D. Fell, M. Sokuler, A. Lembach, T.F. Eibach, C. Liu, E. Bonaccurso, G.K. Auernhammer, H.-J. Butt, Drop impact on surfactant films and solutions, Colloid Polym. Sci. 291 (2013) 1963–1976. doi:10.1007/s00396-013-2931-z.

[5] A.L. Yarin, DROP IMPACT DYNAMICS: Splashing, Spreading, Receding, Bouncing…, Annu. Rev. Fluid Mech. 38 (2006) 159–192. doi:10.1146/annurev.fluid.38.050304.092144.

[6] T. Gilet, J.W.M. Bush, Droplets bouncing on a wet, inclined surface, Phys. Fluids. 24 (2012) 122103. doi:10.1063/1.4771605.

[7] J. Moláček, J.W.M. Bush, Drops bouncing on a vibrating bath, J. Fluid Mech. 727 (2013) 582–611. doi:10.1017/jfm.2013.279.
[8] S.L. Manzello, J.C. Yang, An experimental study of a water droplet impinging on a liquid surface, Exp. Fluids. 32 (2002) 580–589. doi:10.1007/s00348-001-0401-8.
[9] T. Gilet, L. Bourouiba, Fluid fragmentation shapes rain-induced foliar disease transmission, J. R. Soc. Interface. 12 (2015) 20141092–20141092. doi:10.1098/rsif.2014.1092.
[10] M. Massinon, F. Lebeau, Experimental method for the assessment of agricultural spray retention based on high-speed imaging of drop impact on a synthetic superhydrophobic surface, Biosyst. Eng. 112 (2012) 56–64. doi:10.1016/j.biosystemseng.2012.02.005.
[11] L. Mishchenko, B. Hatton, V. Bahadur, J.A. Taylor, T. Krupenkin, J. Aizenberg, Design of Ice-free Nanostructured Surfaces Based on Repulsion of Impacting Water Droplets, ACS Nano. 4 (2010) 7699–7707. doi:10.1021/nn102557p.
[12] W. Jia, H.-H. Qiu, Experimental investigation of droplet dynamics and heat transfer in spray cooling, Exp. Therm. Fluid Sci. 27 (2003) 829–838. doi:10.1016/S0894-1777(03)00015-3.
[13] S.-S. Hsieh, S.-Y. Luo, Droplet impact dynamics and transient heat transfer of a micro spray system for power electronics devices, Int. J. Heat Mass Transf. 92 (2016) 190–205. doi:10.1016/j.ijheatmasstransfer.2015.08.099.
[14] K.B. Subrahmanyam, K.R.V. Kaza, Vibration analysis of rotating turbomachinery blades by an improved finite difference method, Int. J. Numer. Methods Eng. 21 (1985) 1871–1886. doi:10.1002/nme.1620211011.
[15] M.E. Schaffer, A practical guide to noise and vibration control for HVAC systems, 2nd ed, American Society of Heating, Refrigerating, and Air-Conditioning Engineers, Atlanta, GA, 2011.
[16] N.S. Ha, Q.T. Truong, N.S. Goo, H.C. Park, Relationship between wingbeat frequency and resonant frequency of the wing in insects, Bioinspir. Biomim. 8 (2013) 046008. doi:10.1088/1748-3182/8/4/046008.
[17] M.J. Griffin, Discomfort from feeling vehicle vibration, Veh. Syst. Dyn. 45 (2007) 679–698. doi:10.1080/00423110701422426.
[18] M. Brothier, D. Moulinier, C. Bertaux, Drop Impact on a Vibrated, Heated Surface: Towards a Potential New Way of Elaborating Nuclear Fuel from Gel Microspheres, World Acad. Sci. Eng. Technol. Int. J. Chem. Mol. Nucl. Mater. Metall. Eng. 6 (2012) 238–246.
[19] D. Terwagne, F. Ludewig, N. Vandewalle, S. Dorbolo, The role of the droplet deformations in the bouncing droplet dynamics, Phys. Fluids. 25 (2013) 122101. doi:10.1063/1.4832975.
[20] B.T. Ng, Y.M. Hung, M.K. Tan, Suppression of the Leidenfrost effect via low frequency vibrations, Soft Matter. 11 (2015) 775–784. doi:10.1039/C4SM02272F.
[21] H.J. Lee, H.-Y. Kim, Control of drop rebound with solid target motion, Phys. Fluids. 16 (2004) 3715. doi:10.1063/1.1787842.
[22] K.A. Raman, R.K. Jaiman, Y. Sui, T.-S. Lee, H.-T. Low, Rebound suppression of a droplet impacting on an oscillating horizontal surface, Phys. Rev. E. 94 (2016). doi:10.1103/PhysRevE.94.023108.
[23] X. Li, X. Ma, Z. Lan, Dynamic Behavior of the Water Droplet Impact on a Textured Hydrophobic/Superhydrophobic Surface: The Effect of the Remaining Liquid Film Arising on the Pillars' Tops on the Contact Time, Langmuir. 26 (2010) 4831–4838. doi:10.1021/la903603z.
[24] L. Xu, W.W. Zhang, S.R. Nagel, Drop Splashing on a Dry Smooth Surface, Phys. Rev. Lett. 94 (2005). doi:10.1103/PhysRevLett.94.184505.
[25] M. Ebrahim, A. Ortega, Identification of the impact regimes of a liquid droplet propelled by a gas stream impinging onto a dry surface at moderate to high Weber number, Exp. Therm. Fluid Sci. 80 (2017) 168–180. doi:10.1016/j.expthermflusci.2016.08.019.
[26] P.B. Weisensee, J. Tian, N. Miljkovic, W.P. King, Water droplet impact on elastic superhydrophobic surfaces, Sci. Rep. 6 (2016) 30328. doi:10.1038/srep30328.

[27] See Supplemental Material at [URL] for videos, and additional experimental results., (n.d.).
[28] D. Richard, C. Clanet, D. Quéré, Surface phenomena: Contact time of a bouncing drop, Nature. 417 (2002) 811–811. doi:10.1038/417811a.
[29] J.C. Bird, S.S.H. Tsai, H.A. Stone, Inclined to splash: triggering and inhibiting a splash with tangential velocity, New J. Phys. 11 (2009) 063017. doi:10.1088/1367-2630/11/6/063017.
[30] D.G.K. Aboud, A.-M. Kietzig, Splashing Threshold of Oblique Droplet Impacts on Surfaces of Various Wettability, Langmuir. 31 (2015) 10100–10111. doi:10.1021/acs.langmuir.5b02447.
[31] C. Antonini, F. Villa, M. Marengo, Oblique impacts of water drops onto hydrophobic and superhydrophobic surfaces: outcomes, timing, and rebound maps, Exp. Fluids. 55 (2014). doi:10.1007/s00348-014-1713-9.
[32] E. Dressaire, A. Sauret, F. Boulogne, H.A. Stone, Drop impact on a flexible fiber, Soft Matter. 12 (2016) 200–208. doi:10.1039/C5SM02246K.
[33] J.T. Pearson, D. Maynes, B.W. Webb, Droplet impact dynamics for two liquids impinging on anisotropic superhydrophobic surfaces, Exp. Fluids. 53 (2012) 603–618. doi:10.1007/s00348-012-1320-6.
[34] H. Hu, L. Chen, S. Huang, B. Song, Rebound behaviors of droplets impacting on a superhydrophobic surface, Sci. China Phys. Mech. Astron. 56 (2013) 960–965. doi:10.1007/s11433-012-4968-2.
[35] J. Moláček, J.W.M. Bush, Drops walking on a vibrating bath: towards a hydrodynamic pilot-wave theory, J. Fluid Mech. 727 (2013) 612–647. doi:10.1017/jfm.2013.280.
[36] S. Dorbolo, D. Terwagne, N. Vandewalle, T. Gilet, Resonant and rolling droplet, New J. Phys. 10 (2008) 113021. doi:10.1088/1367-2630/10/11/113021.
[37] M. Hubert, D. Robert, H. Caps, S. Dorbolo, N. Vandewalle, Resonant and antiresonant bouncing droplets, Phys. Rev. E. 91 (2015). doi:10.1103/PhysRevE.91.023017.
[38] D.B. van Dam, C. Le Clerc, Experimental study of the impact of an ink-jet printed droplet on a solid substrate, Phys. Fluids. 16 (2004) 3403–3414. doi:10.1063/1.1773551.
[39] K. Okumura, F. Chevy, D. Richard, D. Quéré, C. Clanet, Water spring: A model for bouncing drops, Europhys. Lett. EPL. 62 (2003) 237–243. doi:10.1209/epl/i2003-00340-1.
[40] H.-Y. Kim, J.-H. Chun, The recoiling of liquid droplets upon collision with solid surfaces, Phys. Fluids. 13 (2001) 643–659. doi:10.1063/1.1344183.
[41] G.B. Footte, The Water Drop Rebound Problem: Dynamics of Collision, J. Atmospheric Sci. 32 (1975) 390–402. doi:10.1175/1520-0469(1975)032<0390:TWDRPD>2.0.CO;2.
[42] T. Gilet, J.W.M. Bush, Chaotic Bouncing of a Droplet on a Soap Film, Phys. Rev. Lett. 102 (2009). doi:10.1103/PhysRevLett.102.014501.
[43] T. Gilet, N. Vandewalle, S. Dorbolo, Controlling the partial coalescence of a droplet on a vertically vibrated bath, Phys. Rev. E. 76 (2007). doi:10.1103/PhysRevE.76.035302.
[44] T. Vasileiou, J. Gerber, J. Prautzsch, T.M. Schutzius, D. Poulikakos, Superhydrophobicity enhancement through substrate flexibility, Proc. Natl. Acad. Sci. (2016) 201611631. doi:10.1073/pnas.1611631113.
[45] R.B. Cocroft, R.L. Rodríguez, The Behavioral Ecology of Insect Vibrational Communication, BioScience. 55 (2005) 323. doi:10.1641/0006-3568(2005)055[0323:TBEOIV]2.0.CO;2.
[46] R.F. Chapman, S.J. Simpson, A.E. Douglas, The insects: structure and function, Fifth edition, Cambridge University Press, New York, 2013.